

---

# Stitched ViTs are Flexible Vision Backbones

---

Zizheng Pan Jing Liu Haoyu He Jianfei Cai Bohan Zhuang<sup>†</sup>

ZIP Lab, Monash University, Australia

## Abstract

Large pretrained plain vision Transformers (ViTs) have been the workhorse for many downstream tasks. However, existing works utilizing off-the-shelf ViTs are inefficient in terms of training and deployment, because adopting ViTs with individual sizes requires separate training and is restricted by fixed performance-efficiency trade-offs. In this paper, we are inspired by stitchable neural networks, which is a new framework that cheaply produces a single model that covers rich subnetworks by stitching pretrained model families, supporting diverse performance-efficiency trade-offs at runtime. Building upon this foundation, we introduce SN-Netv2, a systematically improved model stitching framework to facilitate downstream task adaptation. Specifically, we first propose a Two-way stitching scheme to enlarge the stitching space. We then design a resource-constrained sampling strategy that takes into account the underlying FLOPs distributions in the space for improved sampling. Finally, we observe that learning stitching layers is a low-rank update, which plays an essential role on downstream tasks to stabilize training and ensure a good Pareto frontier. With extensive experiments on ImageNet-1K, ADE20K, COCO-Stuff-10K, NYUv2 and COCO-2017, SN-Netv2 demonstrates strong ability to serve as a flexible vision backbone, achieving great advantages in both training efficiency and adaptation. Code will be released at <https://github.com/ziplab/SN-Netv2>.

## 1 Introduction

General-purpose Transformer architectures [3, 15, 12, 53, 26, 5] have grown into unprecedented scale in recent research. In computer vision, large pretrained plain ViTs such as MAE [20], DINO [5, 32] and DeiT [44, 45] are widely adopted as backbones for tackling downstream tasks. However, despite the great performance, when adopting pretrained ViTs into the downstream tasks, they all face the challenge of the huge computational and memory cost. For example, processing a single  $224 \times 224$  image using DeiT3-Large [45] requires 2.8G peak GPU memory consumption, which is  $14\times$  higher than that of using DeiT3-Small (0.2G).

On the other hand, most existing efforts adopting Transformers as backbones for downstream tasks can be roughly categorised into three types of approaches: full-adoption [28, 56, 42, 16], parameter-efficient tuning [24, 7] and adapters [9]. Specifically, full-adoption trains one scale of ViT on downstream tasks while parameter-efficient methods additionally reduce the number of learnable parameters. Adapter method like ViT-Adapter [9] equips plain ViTs with pyramid feature maps for dense predictions. However, these methods do not address the memory consumption and computational cost after adoption.

Most recently, a promising framework has been proposed named stitchable neural networks (SN-Netv1, Figure 2 (a)) [33], where it reassembles a new network (stitch) by stitching pretrained model families (anchors) in a Fast-to-Slow direction, *i.e.*, the stitch begins with a small ViT and goes into a large ViT via a stitching layer ( $1 \times 1$  convolution). At training time, SN-Net randomly samples a stitch and train it as a normal network with gradient descent. With a few epochs of finetuning

---

<sup>†</sup>Corresponding author. E-mail: bohan.zhuang@gmail.com

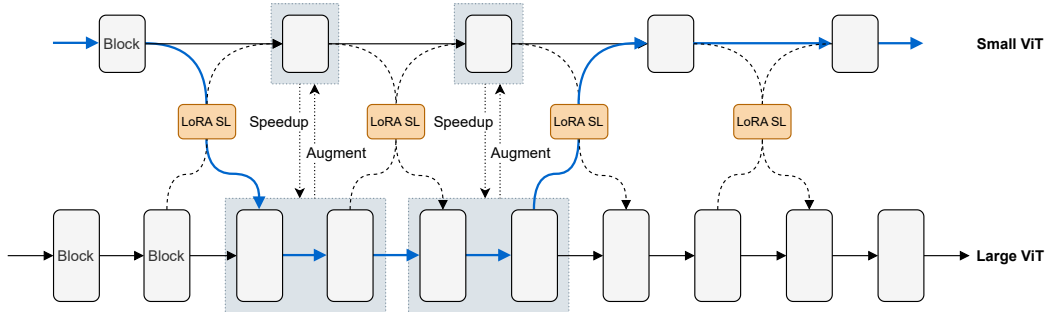


Figure 1: The framework of the proposed Two-way Stitching, where stitching can go Fast-to-Slow, Slow-to-Fast, or travel between anchors as a round trip. For example, the blue line represents the forward path of a new stitched network, which starts with blocks from the small ViT, connects a few blocks from the large ViT, and finally propagates its activations back to the small ViT. “LoRA SL” refers to the proposed low-rank adaptation of stitching layers.

on the same pretraining dataset (*i.e.*, ImageNet-1K), SN-Netv1 produces numerous networks with different performance-efficiency trade-offs that satisfy various resource constraints. However, many general-purpose ViTs are trained on exceptionally large datasets (*e.g.*, JFT [53], LAION [39]) by industry, making it impractical for researchers to train SN-Netv1 on the same domain as the anchors. Therefore, exploring the downstream adaptation of SN-Net becomes essential as it enables researchers to use off-the-shelf pretrained models without significant retraining overhead on the original dataset.

In this paper, we systematically improve SN-Netv1 for direct adaptation on downstream dense predictions. The new method, called **SN-Netv2**, presents impressive power as a strong and flexible vision backbone on downstream CV tasks. Specifically, our improvements are in three folds: 1) Different from SN-Netv1 that only permits the stitching direction of Fast-to-Slow, we propose a novel Two-way stitching strategy (Figure 1), which enables stitching to go both Fast-to-Slow and Slow-to-Fast, or travel between anchors as a round trip (*e.g.*, Fast-Slow-Fast). As a result, we effectively enlarge the stitching space by  $10\times$  and avoid sub-optimal stitches that reside in certain resource constraints. However, under the default random sampling strategy, simply enlarging the space incurs unbalanced training and hinders the overall performance of SN-Netv1 due to the varying number of stitches residing on different FLOPs intervals. To this end, 2) we introduce a Resource-constrained Sampling (ROS) strategy, which draws a stitch at each iteration according to the categorical distribution of stitches in the space [46, 30]. In this case, ROS ensures a balanced training for stitches under different resource constraints. 3) Last, although SN-Netv1 demonstrated the advantage of fully finetuning the stitching layers after least-square initialization, we point out that learning stitching layers resides on a low intrinsic dimension. On ImageNet-1K, low-rank adaptation of stitching layers achieves competitive performance, while it plays a key role in stabilizing training and ensuring a smooth performance curve on downstream tasks.

With the improved techniques, we comprehensively experiment with SN-Netv2 on ImageNet-1K, ADE20K, COCO-Stuff-10K, NYUv2 and COCO. We show SN-Netv2 demonstrates strong performance and training efficiency than typical single-scale ViT backbone adoption on downstream dense prediction tasks. In particular, on ImageNet-1K, SN-Netv2 obtains better performance-efficiency trade-offs than SN-Netv1. On downstream tasks, SN-Netv2 achieves competitive performance with anchors under equal training schedules, while eliminating the need to train different scales of ViT backbone separately. With systematic evaluation, we show SN-Netv2 enables flexible inference on memory and computation-intensive dense predictions with a single network, showcasing its potential as a next-generation backbone for a wide range of tasks.

## 2 Related Work

**General-purpose Transformers.** Benefit from the large-scale datasets [39, 53] and powerful scaling laws [25], recent pretrained plain ViTs [20, 2, 14, 12] have achieved strong performance on many visual benchmarks. Based on different training objectives, ViT pretraining can be done by either supervised learning (SL) or self-supervised learning (SSL). In SL-based pretraining, the common practice [31, 14] is to train ViTs with the cross-entropy loss on ImageNet-21K [38] or

privately gathered images [43]. Compared to it, SSL-based pretraining is a more promising direction as it can leverage the vast amounts of unlabeled data. Prevalent approaches in this area include contrastive learning [5, 8, 52, 35] and masked image modeling (MIM) [20, 2, 58, 13, 18, 50]. In recent studies, ViTs have been scaled up to billion parameters [53, 12, 15] to match the prevalent large language models (LLMs) [55, 36, 3]. However, when adopting into downstream tasks, most existing efforts [28, 16, 54, 56] fully adopt the pretrained model in order to exploit the pretrained weights, suffering from the huge computational cost and memory consumption. In contrast, this paper efficiently adapts large pretrained ViTs into CV tasks as a single flexible backbone to satisfy various resource constraints at runtime.

**Model stitching.** Model stitching has been studied in previous works [27, 1, 11] to measure the similarity of representations from neural networks. In particular, it implies a sequence of well-performed networks that can be obtained by stitching the early portion of a trained network with the last portion of another trained network by a  $1 \times 1$  convolution layer (a.k.a, stitching layer). Inspired by this observation, Yang *et al.* [51] proposed to dissect and reassemble a new architecture based on the model zoo. Most recently, Pan *et al.* proposed SN-Net [33] to cheaply produce numerous networks with different complexity-performance trade-offs by stitching a family of pretrained models. However, it only experiments with the same pretraining domain, without exploring dense prediction performance. In this paper, we systematically improves SN-Net and address its limitations on the stitching space, sampling strategy and downstream training adaptation.

### 3 Rethinking Stitchable Neural Networks

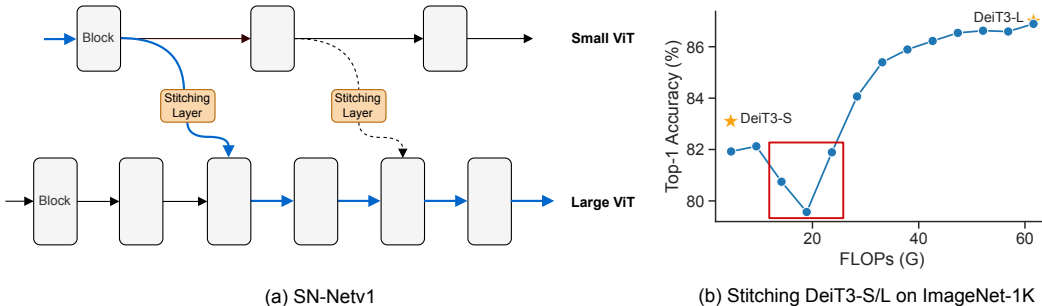


Figure 2: Explanation of SN-Netv1 [33]. Figure (a): The framework of SN-Netv1 under the default Fast-to-Slow strategy, where the blue line indicates the forward path of a stitched network by stitching a small ViT to a large ViT. Figure (b): The naive Fast-to-Slow stitching strategy incurs some bad stitches (highlight in red box) when stitching pretrained DeiT3-S and DeiT3-L on ImageNet-1K.

SN-Netv1 [33] is a scalable framework built upon pretrained model families. A simple illustration of SN-Netv1 is shown in Figure 2 (a). Specifically, given an input  $\mathbf{X}$  and two pretrained models  $f_\theta$  and  $f_\phi$ ,  $\mathcal{S} : \mathcal{A}_{\theta,l} \rightarrow \mathcal{A}_{\phi,m}$  is denoted as a stitching layer which implements a transformation between the activation space of the  $l$ -th layer of  $f_\theta$  to the activation space of the  $m$ -th layer of  $f_\phi$ . Let  $Z_\theta$  and  $G_\phi$  represent the function of the first and last portion of blocks of  $f_\theta$  and  $f_\phi$  respectively. Next, SN-Netv1 obtains a new network architecture  $F_S$  by

$$F_S(\mathbf{X}) = G_{\phi,m} \circ \mathcal{S} \circ Z_{\theta,l}(\mathbf{X}), \quad (1)$$

where  $\circ$  indicates the composition. With different stitching configurations of  $l$  and  $m$ , SN-Net cheaply produces numerous stitched networks (*i.e.*, stitches) that achieve good accuracy-efficiency trade-offs between two pretrained models (*i.e.*, anchors) after joint training. However, despite the simple idea and its effectiveness, SN-Net still suffers from noticeable limitations.

**Stitching space.** SN-Netv1 strictly follows a typical stitching direction in the literature [1, 11], *i.e.*, propagating activations by starting with one anchor and ending with another. Based on whether the stitched network starts with a small anchor (Fast) or a large anchor (Slow), Pan *et al.* [33] explored two stitching directions: Fast-to-Slow and Slow-to-Fast, and demonstrated that Fast-to-Slow generally leads to a better and more smooth performance curve. However, simply adhering to the Fast-to-Slow direction may assemble sub-optimal network architectures. As shown in Figure 2 (b), stitching DeiT3-S and DeiT3-L under the default setting of SN-Netv1 produces a few stitches that

achieve worse performance than the small anchor, even with higher FLOPs. Therefore, it is evident that the existing stitching space in SN-Netv1 requires redesign.

**Sampling strategy.** Training SN-Netv1 is simple but effective: at each training iteration, SN-Netv1 randomly samples a stitch from a pre-defined configuration set, and then train the sampled stitch as a normal network with gradient descent. However, random sampling approach only works well when the stitches are evenly distributed across different FLOPs constraints (*e.g.*, 5G, 10G). While this condition is met in the initial stitching space of SN-Netv1, enlarging the space can result in a problematic imbalance, with some FLOPs constraints having far fewer stitches than others. Consequently, this leads to an unbalanced training for networks in certain FLOPs ranges, and thus negatively impacts the performance.

**Stitching layers.** SN-Netv1 is initially trained on the same data source of the pretrained model families (*e.g.*, ImageNet-1K pretrained DeiT3 [44]). Under this setting, training a stitching layer with fully finetuning has a consistent target as the activation space  $\mathcal{A}_{\theta,l}$  and  $\mathcal{A}_{\phi,m}$  may not change significantly. However, things can be different when adopting SN-Netv1 on downstream dense prediction tasks due to the domain gap between the pretrained data and the target data. In this case, both  $\mathcal{A}_{\theta,l}$  and  $\mathcal{A}_{\phi,m}$  need to adapt to the target domain, making it unstable and difficult to simultaneously learn many stitches. This implies the necessity of an appropriate method for learning stitching layers on downstream tasks.

## 4 Method

In this section, we systematically introduce our improvements over SN-Netv1, including the redesign of stitching space, sampling strategy and stitching layers for stable adaptation to downstream dense prediction tasks.

### 4.1 Two-way Stitching

To improve the stitching space, we first propose Two-way stitching, which allows the stitching to travel in different ways including Fast-to-Slow (FS), Slow-to-Fast (SF), Fast-Slow-Fast (FSF) and Slow-Fast-Slow (SFS). The design principle of Two-way Stitching is to augment the small anchor with the blocks from a large and strong anchor, while accelerating the large anchor by adopting more efficient blocks from the small anchor. In this way, Two-way stitching can leverage the strengths of different scales of anchors.

We illustrate our framework in Figure 1, where it also shows a concrete example of an FSF stitch in the blue line of Figure 1. Specifically, its begins with the small anchor during the forwarding pass, traverses the large anchor along the middle route, and ultimately returns to the small anchor for subsequent propagations. By enabling a broader stitching configuration, Two-way stitching enlarges the stitching space by  $10\times$  compared to the initial space of SN-Netv1 (*e.g.*, 134 *vs.* 13 based on DeiT3-S/L), which facilitates the discovery of more optimal architectures, as shown in Section 5. Moreover, benefiting from the two new stitching configurations (*i.e.*, FSF and SFS), SN-Netv2 can produce many networks at the similar FLOPs as each stitch can be regarded as replacing intermediate consecutive blocks at certain positions in one anchor with the blocks from another anchor.

### 4.2 Resource-Constrained Sampling

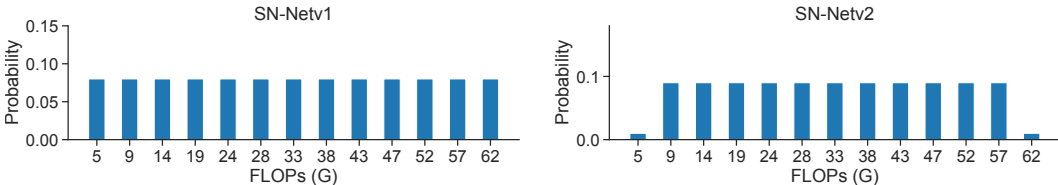


Figure 3: Comparison on the categorical distribution of stitches between SN-Netv1 and SN-Netv2 by stitching DeiT3-S and DeiT3-L on ImageNet-1K.

After enlarging the stitching space, we empirically find that the performance of anchors drops significantly compared to its original performance. To understand this, we begin with analysing the categorical distribution of stitches in the space, *i.e.*,  $\pi(\tau)$ , where  $\tau$  denotes the FLOPs constraint. In

practice, we round the real FLOPs following a step  $t$  to discretize the whole FLOPs range. By default, we adopt  $t = 1$  in ImageNet experiments and  $t = 10$  for dense prediction tasks. Benefiting from the significantly smaller architectural space compared to neural architecture search (*i.e.*, NAS,  $10^2$  vs.  $10^{20}$ ), we can calculate  $\pi(\tau)$  exactly prior to training by  $\pi(\tau = \tau_0) = \#(\tau = \tau_0)/E$ , where  $E$  is the total number of stitches in the space and  $\#(\tau = \tau_0)$  is the number of stitches that yield FLOPs  $\tau_0$ .

With the exact  $\pi(\tau)$ , we visualize the categorical distribution of stitches for SN-Netv2 and SN-Netv1 in Figure 3. As it shows, stitches in SN-Netv1 are evenly distributed across different FLOPs, which ensures balanced training for stitches at different resource constraints. However, under Two-way Stitching, the sampling probability of anchors (2/134) is much lower than stitches in other FLOPs constraints. As a result, anchors are significantly under-trained which therefore affects the overall performance of SN-Netv2. Inspired by recent NAS works [46, 30], we design a Resource-constrained Sampling strategy (ROS) for SN-Netv2. Specifically, at each training iteration, we first sample a FLOPs constraint  $\tau_0$ . Next, we randomly sample a stitch that satisfies the constraint  $\alpha \sim \pi(\tau = \tau_0)$ . With this design, ROS effectively guarantees balanced training for stitches at different FLOPs constraints, especially for anchors where we increase their sampling probability by  $10\times$ , *e.g.*, from 2/134 to 2/13 based on DeiT3-S/L and 13 FLOPs intervals.

### 4.3 Low-Rank Adaptation of Stitching Layers

Under Two-way stitching, the stitching layers involve with two types of transformation matrix to control how the stitches route between anchors:  $\mathbf{M}_1 \in \mathbb{R}^{D_1 \times D_2}$  and  $\mathbf{M}_2 \in \mathbb{R}^{D_2 \times D_1}$ , where  $D_1$  and  $D_2$  refer to model widths of the small anchor and large anchor, respectively. In practice, they are  $1 \times 1$  convolutions and initialized by the least-square (LS) solution as in SN-Netv1. Formally, let  $\mathbf{X}_1 \in \mathbb{R}^{N \times D_1}$  and  $\mathbf{X}_2 \in \mathbb{R}^{N \times D_2}$  be the feature maps from two anchors at one stitching position, where  $N$  denotes the length of the input sequence. Next, the targeted transformation matrix for  $\mathcal{S}_1$  and  $\mathcal{S}_2$  can be obtained respectively by

$$\mathbf{M}_1 = \mathbf{X}_1^\dagger \mathbf{X}_2, \mathbf{M}_2 = \mathbf{X}_2^\dagger \mathbf{X}_1, \quad (2)$$

where  $\dagger$  denotes the Moore-Penrose pseudoinverse of a matrix. In SN-Netv1, the transformation matrix  $\mathbf{M}$  is fully finetuned with gradient descent during training, which demonstrates better performance than the initial LS solution.

However, as mentioned in Section 3, learning a good stitching layer on downstream tasks can be difficult as anchors need to adapt to the target domain simultaneously. Motivated by previous observations [17, 6] that sparse finetuning via parameter-efficient tuning (PET) can impose regularization on the model which facilitates training stability, we propose LoRA SL, a low-rank adaptation method for stitching layers in order to stabilize training. Specifically, similar to LoRA [23], we freeze the LS initialized transformation matrix  $\mathbf{M}$  but constrain its update with a low-rank decomposition. Taking  $\mathcal{S}_1$  as a concrete example, the activation projection of the stitching layer can be formulated by

$$\mathbf{X}_1 \mathbf{M}_1 + \mathbf{X}_1 \Delta \mathbf{M}_1 = \mathbf{X}_1 \mathbf{M}_1 + \mathbf{X}_1 \mathbf{B}_1 \mathbf{A}_1, \quad (3)$$

where  $\mathbf{B}_1 \in \mathbb{R}^{D_1 \times r}$ ,  $\mathbf{A}_1 \in \mathbb{R}^{r \times D_2}$ , and  $r \ll \min(D_1, D_2)$  is the rank. In practice,  $\mathbf{B}_1$  is initialized by Gaussian initialization and  $\mathbf{A}_1$  is initialized with zeros. Therefore, the initial update  $\Delta \mathbf{M}_1 = \mathbf{B}_1 \mathbf{A}_1$  is zero and does not affect the LS solution at the beginning of training. As each stitching layer is responsible for multiple stitches, the low-rank update helps to regularize the learning of  $\mathbf{M}_1$ . We show in Figure 11 that LoRA SL improves the overall performance of SN-Netv2. In Algorithm 1, we summarize our training approach for SN-Netv2 and highlight the difference with SN-Netv1 in bold. It is also worth noting that we do not adopt knowledge distillation to train SN-Netv2 as it is very inefficient on downstream dense prediction tasks.

## 5 Experiments

In this section, we first show the advantage of SN-Netv2 over SN-Netv1 on ImageNet-1K [38]. Next, we conduct experiments on downstream dense prediction tasks to show the strong performance of SN-Netv2 as a promising flexible vision backbone, including semantic segmentation on ADE20K [57], COCO-Stuff [4], depth estimation on NYUv2 [40] and object detection on COCO-2017 [29].

---

**Algorithm 1** Training Stitchable Neural Networks v2

---

**Require:** Two pretrained ViTs to be stitched. **The pre-computed categorical distribution of stitches in the Two-way stitching space  $\pi(\tau)$ .**

- 1: Initialize all stitching layers by least-squares matching, **freeze the weights M with LoRA.**
  - 2: **for**  $i = 1, \dots, n_{iters}$  **do**
  - 3:   Get next mini-batch of data  $\mathbf{X}$  and label  $\mathbf{Y}$ .
  - 4:   Clear gradients, `optimizer.zero_grad()`.
  - 5:   **Sample a target resource constraint  $\tau_0$ .**
  - 6:   **Randomly sample a stitch  $\alpha$  that satisfies the constraint  $\alpha \sim \pi(\tau = \tau_0)$ .**
  - 7:   Execute the current stitch,  $\hat{\mathbf{Y}} = F_\alpha(\mathbf{X})$ .
  - 8:   Compute loss,  $loss = criterion(\hat{\mathbf{Y}}, \mathbf{Y})$ .
  - 9:   Compute gradients, `loss.backward()`.
  - 10:   Update weights, `optimizer.step()`.
  - 11: **end for**
- 

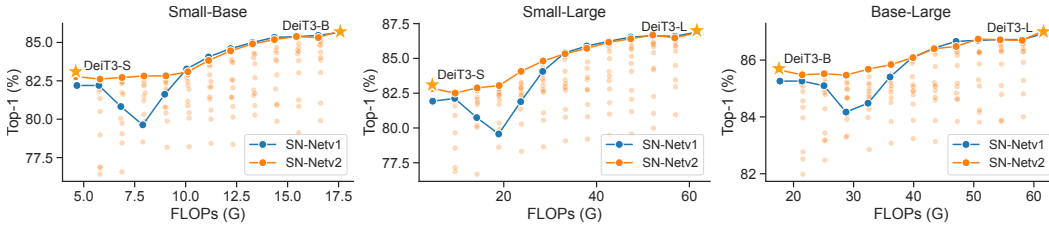


Figure 4: Performance comparison between SN-Netv1 and SN-Netv2 on ImageNet-1K based on DeiT3. The yellow stars denote the original anchor performance. We highlight the best performed stitches on the Pareto-frontier in SN-Netv2.

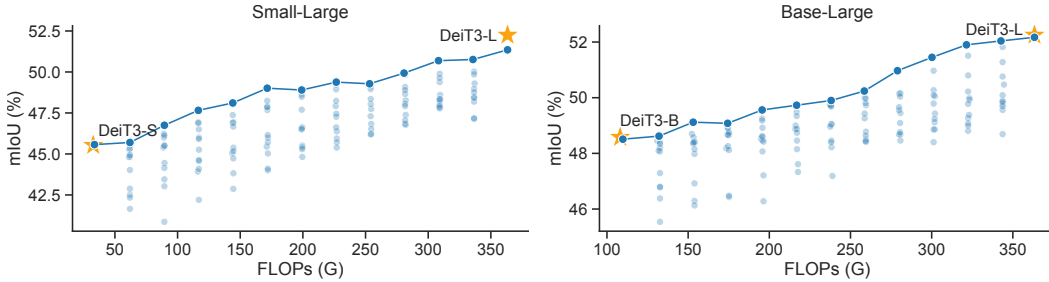


Figure 5: Semantic segmentation results of SN-Netv2 on ADE20K by stitching DeiT3-S/L and DeiT3-B/L. We use yellow stars to denote the anchor performance, *i.e.*, adopt the individual anchor as a backbone for training. We highlight the stitches at the Pareto frontier in blue line.

## 5.1 ImageNet Classification

**Implementation details.** We experiment with three combinations of stitching for DeiT3 [45], namely DeiT3-S/B, DeiT3-S/L and DeiT3-B/L. We train each setting on ImageNet-1K by 30 epochs with a total batch size of 256 on 8 V100 GPUs. The learning rate is  $0.1 \times$  to that of default training time learning rate in DeiT3. During training, anchors adopt the same stochastic layer drop rate as the pretrained model family, *i.e.*, 0.05, 0.15, 0.4 for DeiT3-S, DeiT3-B, DeiT3-L, respectively. All other hyperparameters are the same as in DeiT3. For all experiments, we adopt a rank of 16 for LoRA SL and 100 images for its LS initialization. We evaluate the performance by Top-1 accuracy (%).

**Results.** In Figure 4, we compare SN-Netv2 to SN-Netv1 on ImageNet-1K. With the same training schedule, SN-Netv2 produces hundreds of stitches that satisfy a diverse range of resource constraints. More importantly, by highlighting the stitches on the Pareto frontier, we show SN-Netv2 can find much better architectures, *i.e.*, stitching configurations than SN-Netv1. This is achieved by the enlarged stitching space from Two-way stitching, the improved ROS sampling, as well as the effective low-rank update of stitching layers under LoRA SL. Moreover, while SN-Netv1 results in a noticeable performance drop for the small anchor, SN-Netv2 escapes from the sub-optimal space at the low-FLOPs constraints and significantly improves the stitches that reside in that range. Overall, this strongly demonstrates the advantage of SN-Netv2 over SN-Netv1.



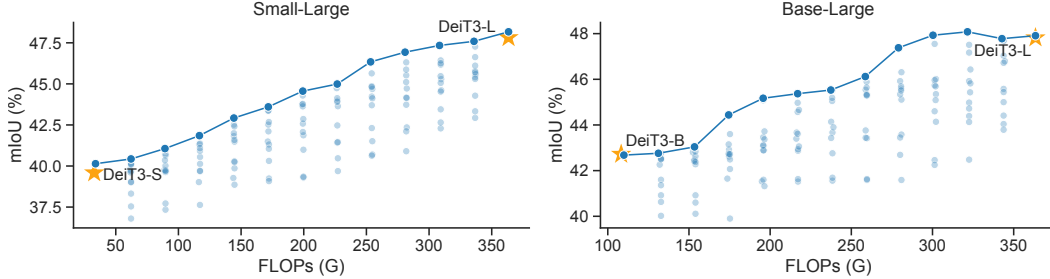


Figure 6: Semantic segmentation results of SN-Netv2 on COCO-Stuff-10K by stitching DeiT3-S/L and DeiT3-B/L. We highlight the stitches at the Pareto frontier in blue line.

Table 1: Training efficiency comparison between SN-Netv2 and individual anchors based on SETR. We measure the training cost by A100 GPU hours. FLOPs and mIoU in SN-Netv2 are represented by a range, *e.g.*, “34 - 363” means the model can cover FLOPs ranging from 34G to 363G.

Model	Params (M)	FLOPs (G)	ADE20K		COCO-Stuff-10K	
			mIoU	Train Cost	mIoU	Train Cost
DeiT3-S	23	32	45.5	75	39.6	40
DeiT3-B	88	108	48.6	90	42.7	48
DeiT3-L	307	363	52.3	174	47.8	90
SN-Netv2 + DeiT3-S/L	338	<b>34 - 363</b>	<b>45.6 - 51.4</b>	<b>120</b>	<b>40.1 - 48.2</b>	<b>60</b>
SN-Netv2 + DeiT3-B/L	412	<b>110 - 363</b>	<b>48.5 - 52.2</b>	<b>140</b>	<b>42.7 - 48.1</b>	<b>80</b>

## 5.2 Semantic Segmentation

**Implementation details.** To explore the power of SN-Netv2 on downstream tasks, we first conduct comprehensive experiments on semantic segmentation, including ADE20K [57] and COCO-Stuff-10K [4]. Our method is based on SETR [56] due to its simple framework which well reflects the performance of plain ViT backbones [54]. It is worth noting that while SETR is proposed along with three different decoders: Naive, PUP and MLA, we adopt the Naive approach as it achieves the best performance-efficiency trade-off. For all experiments, we train with a total batch size of 16 for ADE20K and COCO-Stuff-10K. We set the training iterations as 160K, 80K for ADE20K and COCO-Stuff-10K, respectively. Besides, we adopt a rank of 16 for LoRA SL when stitching DeiT3-S and DeiT3-L, and a rank of 4 for stitching DeiT3-B and DeiT3-L. Similar to ImageNet experiments, we use 100 images for LS initialization. All other hyperparameters are set with default choices in mmsegmentation [10]. Following prior works [49, 54, 19], we adopt mean Intersection over Union (mIoU) as the metric to evaluate the performance.

**ADE20K results.** We report our ADE20K results in Figure 5. Specifically, based on DeiT3-S and DeiT3-L, SN-Netv2 demonstrates strong performance against anchor performance while simultaneously supporting a diverse range of resource constraints. By stitching DeiT3-B and DeiT3-L, SN-Netv2 achieves equal performance with anchors at their FLOPs. Moreover, by plotting the stitches on Pareto Frontier, we show SN-Netv2 smoothly interpolates the performance of two solo backbone settings, which strongly demonstrates the effectiveness of our method.

**COCO-Stuff-10K results.** In Figure 6, we show that stitching DeiT3-S and DeiT3-L under SN-Netv2 even achieves better performance than anchors. More impressively, by stitching DeiT3-B and DeiT3-L, we found some stitches that achieve better performance than the large anchor at a lower FLOPs. It implies that the original plain ViTs may not be the best architecture in different domains.

**Training efficiency.** We demonstrate that SN-Netv2 achieves great training advantages compared to typical backbone adoption in downstream dense prediction tasks. As shown in Table 1, on both ADE20K and COCO-Stuff-10K, stitching DeiT3-S/L or DeiT3-B/L can cover a wide range of performance-efficiency trade-offs in a single network, while requiring even less GPU hours than training the anchors separately (*e.g.*, 140 vs. 174 + 90 on ADE20K).

## 5.3 Depth Estimation

**Implementation details.** Based on DPT [37], we conduct experiments on NYUv2 [40] dataset and train SN-Netv2 by stitching DeiT3-S/L and DeiT3-B/L. Specifically, we train each model on 4 A100

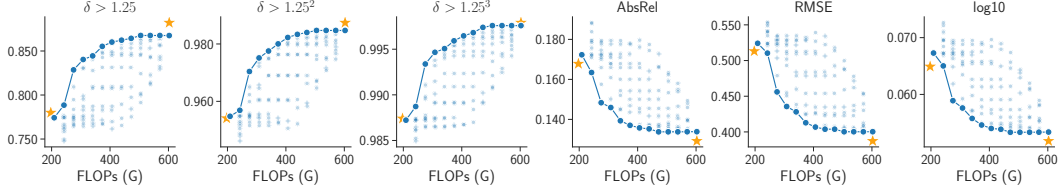


Figure 7: Results of stitching DeiT3-S and DeiT3-L on NYUv2 under the framework of DPT.

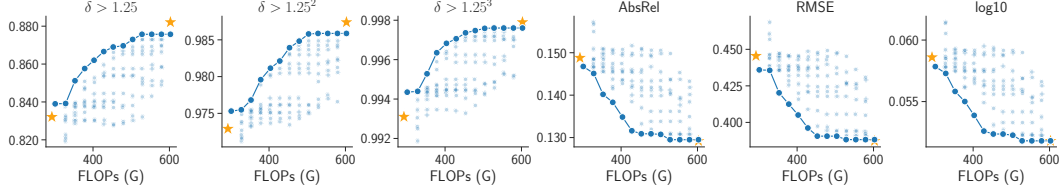


Figure 8: Results of stitching DeiT3-B and DeiT3-L on NYUv2 under the framework of DPT.

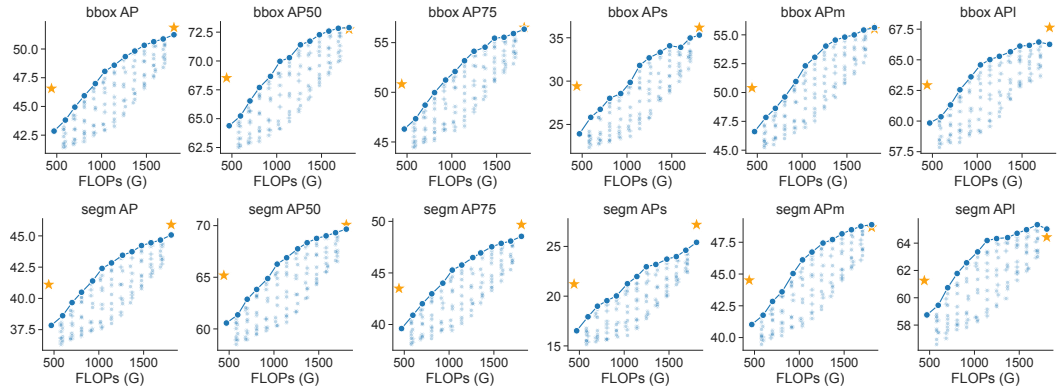


Figure 9: Object detection and instance segmentation results of SN-Netv2 on COCO-2017 by stitching DeiT3-S and DeiT3-L under Mask R-CNN [21] based ViTDet [28]. We report the results on detection metrics in the top row and the instance segmentation metrics in the bottom row.

GPUs with a total batch size of 16. We set the training epochs to 24. We adopt AdamW optimizer with an initial learning rate of  $2 \times 10^{-5}$ . For LoRA SL, we use a rank of 4 for all experiments. We utilize common metrics for evaluating the performance on depth estimation, including  $\delta > 1.25$ ,  $\delta > 1.25^2$ ,  $\delta > 1.25^3$  (where higher values indicate better performance), as well as AbsRel, RMSE, and Log10 (where lower values indicate better performance).

**Results.** We report our experiment results on NYUv2 [40] in Figure 7 and Figure 8. Overall, SN-Netv2 demonstrates highly competitive performance compared to the anchor models, while simultaneously achieving a smooth performance-efficiency curve. In particular, we found stitching DeiT3-B and DeiT3-L is slightly better, which we assume a smaller gap in model complexity between the anchors can help to achieve better performance, which aligns with the observations of SN-Netv1 [33].

#### 5.4 Object Detection and Instance Segmentation

**Implementation details.** We experiment SN-Netv2 on COCO-2017 and adopt Mask R-CNN based ViTDet [28]. We train all models including individual anchors on 8 A100 GPUs with a total batch size of 8 for 100 epochs. We set the rank as 16 for LoRA SL. Besides, we adopt the same layer decay rate as the baselines for different anchors. All other hyperparameters adopt the default setting in detectron2 [47].

**Results.** Based on DeiT3-S and DeiT3-L, we report the performance of SN-Netv2 on object detection and instance segmentation in Figure 9. Overall, we found SN-Netv2 exhibits strong flexibility on the detection task as well, as evidenced by the smooth metrics under various resource constraints. This



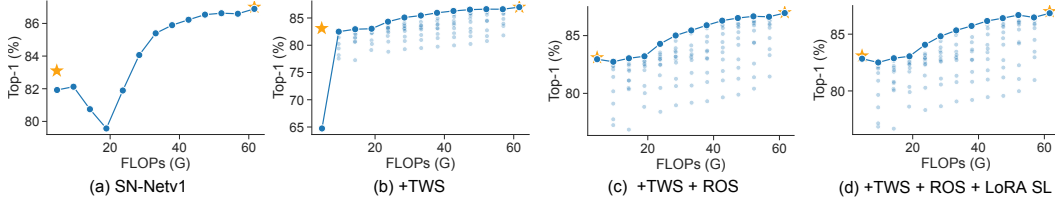


Figure 10: Effect of improvements over SN-Netv1 based on stitching DeiT3-S and DeiT3-L on ImageNet-1K. From left to right, we gradually apply Two-way stitching (TWS), resource-constrained sampling (ROS) and low-rank adaptation of stitching layers (LoRA SL) with a rank of 16.

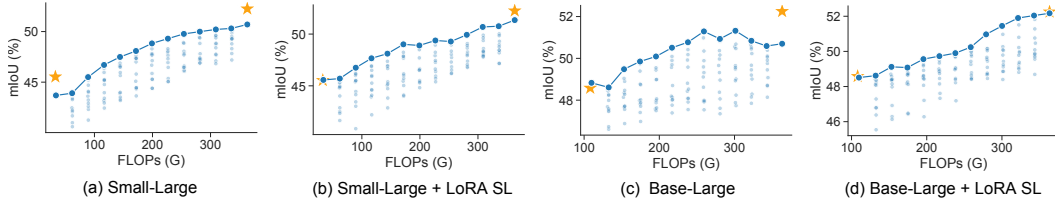


Figure 11: Performance comparison of SN-Netv2 with (Figure (b) and (d)) and without (Figure (a) and (c)) low-rank adaptation for stitching layers on ADE20K.

again demonstrates that SN-Netv2 can serve as a flexible backbone on a wide range of CV tasks. In particular, under the similar training cost ( $\sim 1500$  GPU hours), SN-Netv2 can achieve comparable performance at the FLOPs of individually trained DeiT3-L (51.2 vs. 51.9 bbox AP), while supporting many FLOPs-accuracy trade-offs at runtime without additional training cost. However, we observe a performance gap between individually trained DeiT3-S with that of SN-Netv2 at the same FLOPs (42.9 vs. 46.6 bbox AP). For this, we hypothesize that with the heavy decoder in ViTDet ( $27\times$  larger than SETR decoder), simultaneously ensuring the performance of hundreds of stitches as backbones can be more difficult. Nevertheless, SN-Netv2 still achieves superior advantage in terms of the training efficiency as it only requires training once while covering many FLOPs-accuracy trade-offs. We leave the improvement for future work.

## 5.5 Ablation Study

**Effect of improved techniques.** Based on DeiT3-S and DeiT3-L, we conduct experiments on ImageNet-1K to show the effect of Two-way stitching, resource-constrained sampling and LoRA stitching layers. As shown in Figure 10, benefiting from Two-way stitching, SN-Net successfully finds better stitching configurations at the relatively low FLOPs constraints except for the small anchor where it drops significantly. However, with the help of ROS, we improve the performance of DeiT3-S and therefore ensure the overall performance curve. Finally, we show LoRA SL can achieve comparable performance with the fully finetuned baseline in Figure 10 (c).

**Effect of LoRA SL on downstream tasks.** We have shown that applying SN-Netv2 with or without LoRA SL on ImageNet-1K has a minor effect on the performance. However, we emphasize that low-rank adaptation for stitching layers is critical for ensuring good performance on downstream tasks. In Figure 11, we report the results of SN-Netv2 with/without applying LoRA to stitching layers on ADE20K. As it shows, without LoRA SL, there is a noticeable performance drop for anchors when stitching DeiT3-S/L. The issue is even more pronounced when stitching DeiT3-B/L, resulting in a highly unstable performance curve. However, after applying LoRA to stitching layer, we achieve a more stable and better performance curve. In this case, we speculate that low-rank update of the stitching layer can stabilize anchor learning, thus ensuring good performance of intermediate stitches in SN-Netv2. We show the effect of different ranks in Section A.4.

**Compared to parameter-efficient tuning on backbone.** We investigate the impact of parameter-efficient tuning (PET) on the performance of SN-Netv2 by stitching DeiT3-B/L. Specifically, we apply LoRA with a rank of 4 to the backbone and train it using the same schedule as fully-finetuning on COCO-Stuff-10K. As shown in Figure 12 (a), SN-Netv2 can produce good performance-efficiency trade-offs under PET as well. Moreover, it even achieves better performance than individually trained anchors with PET (e.g., 44.8 vs. 45.8 with DeiT3-L), for which we conjecture SN-Netv2 may regularize the large anchor learning when combining with PET.

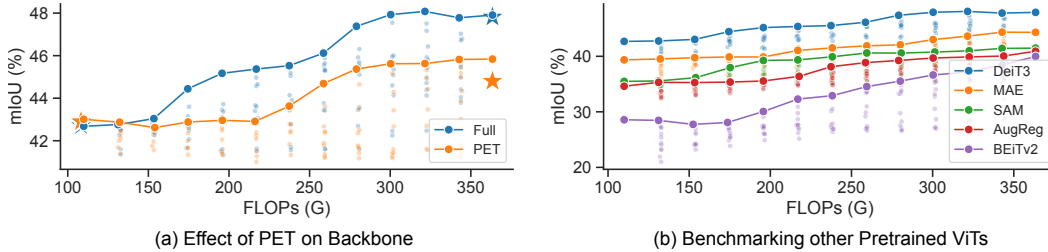


Figure 12: Figure (a): Comparing parameter-efficient tuning (PET) with fully finetuning (Full) on SN-Netv2. Figure (b): Benchmarking different pretrained weights of plain ViTs under SN-Netv2. Experiments are conducted on COCO-Stuff-10K and based on Base/Large variants of ViTs.

**Benchmarking other pretrained ViT weights.** In Figure 12 (b), we report the results of stitching different pretrained weights based on the base and large variants of ViTs, including MAE [20], SAM [26], AugReg [41] and BEiTv2 [34]. Overall, SN-Netv2 consistently generates good Pareto frontiers for these weights. As pre-training objectives and datasets differ across ViTs, our results in Figure 12 (b) demonstrate varying performance when stitching different ViT weights, where DeiT3 achieves the best performance. Therefore, we choose DeiT3 as the default weights.

## 6 Conclusion and Future Work

We have introduced SN-Netv2, a systematically improved training framework that effectively employs off-the-shelf foundation ViTs to obtain a flexible and strong vision backbone on downstream dense prediction tasks. In particular, we have first proposed a Two-way stitching strategy to enlarge the stitching space and effectively identified more optimal stitches in certain resource constraints. Next, we have devised a resource-constrained sampling approach to ensure balanced training for stitches that reside on different resource constraints, thereby enhancing the overall performance of SN-Netv2. Furthermore, we have demonstrated that low-rank adaptation of stitching layers yields competitive performance on ImageNet-1K while playing a crucial role in stabilizing training on downstream tasks. Extensive experiments across various datasets have demonstrated that SN-Netv2 achieves great training efficiency and inference flexibility than typical ViT backbone adoption, benefiting the massive model deployment in real-world applications.

**Limitations and societal impact.** This paper mainly aims to improve SN-Netv1 for flexible ViT adoption on downstream tasks, which however leaves parameter efficient approaches [24, 23, 7] under-explored. Future work may also consider a better training strategy to improve the performance of stitches on the Pareto frontier. Besides, SN-Netv2 requires multi-GPU training, which inevitably results in a substantial electricity consumption and carbon emission.

## A Appendix

We organize our supplementary material as follows.

- In Section A.1, we compare different stitching types at initialization based on ImageNet-1K.
- In Section A.2, we compare different stitching types after training based on ImageNet-1K.
- In Section A.3, we compare SN-Netv2 with SN-Netv1 on semantic segmentation.
- In Section A.4, we explore the effect of different ranks in LoRA SL.
- In Section A.5, we describe the details of the benchmarked pretrained ViTs.

### A.1 Performance Comparisons of Different Stitching Types at Initialization

By default, we randomly sample 100 images from the train set and solve the least-square problem to initialize the stitching layers. After initialization, we directly compare the performance of different types of stitches based on DeiT3 models and ImageNet-1K. Overall, the observations depicted in Figure 13 indicate that Fast-to-Slow (FS) outperforms at high FLOPs, while Slow-to-Fast (SF) excels at low FLOPs. This highlights the effectiveness of Two-way stitching, as no single stitching direction

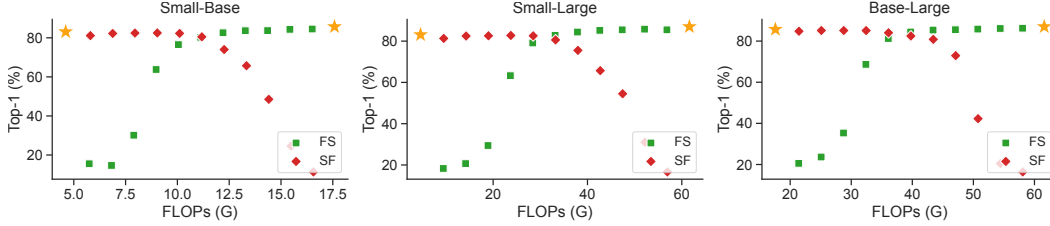


Figure 13: Performance comparison between SF and FS stitches on ImageNet-1K at initialization.

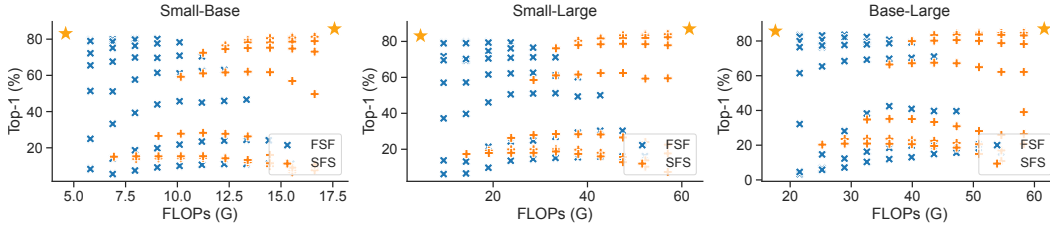


Figure 14: Performance comparison between FSF and SFS stitches on ImageNet-1K at initialization.

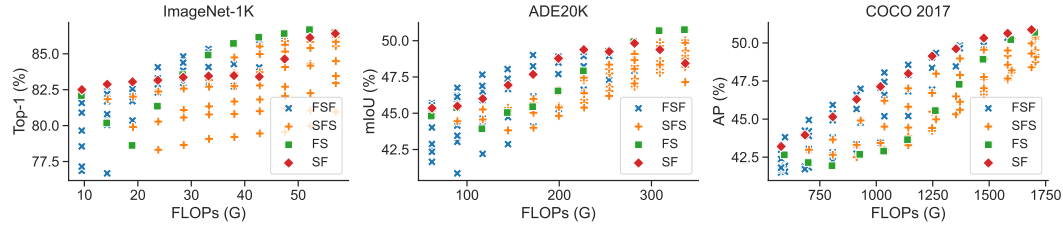


Figure 15: Ranking visualization of different types of stitches on image classification, semantic segmentation and object detection.

emerges as the superior choice across all FLOPs intervals. Similarly, in Figure 14, we find that Fast-Slow-Fast (FSF) generally outperforms Slow-Fast-Slow (SFS) at low FLOPs, whereas SFS stitching prevails at high FLOPs. This implies that benefiting from the enlarged stitching space, SN-Netv2 can find a large number of more optimal architectures than SN-Netv1 (which uses FS only), enabling them to achieve favorable performance right from the initialization phase.

## A.2 Performance Comparison of Different Stitching Types after Training

We show in Figure 15 that different stitching types present varying performance in different resource constraints after training. Similar to the phenomenon in Section A.1, our findings reveal that SF outperforms FS at low FLOPs, while FS becomes superior at high FLOPs, particularly for ImageNet-1K and ADE20K. We attribute this to the fact that networks adopting a few early blocks from the other anchor tend to perform better, indicating that stitching at the early stages of ViTs is more effective when stitched only once. For this, we assume early blocks involve with general low level features [22, 48], which makes them more amenable to stitch. Besides, FSF stitches are generally better than that of SFS after training. These observations can serve as valuable guidelines for future stitching designs.

## A.3 Performance Comparison of SN-Netv1 and SN-Netv2 on Semantic Segmentation

Based on DeiT3-S and DeiT3-L, we compare the performance of SN-Netv2 to SN-Netv1 on ADE20K and COCO-Stuff-10K. By default, we adopt a rank of 16 for LoRA SL and train each model on ADE20K with a 160K schedule and COCO-Stuff-10K with a 80K schedule. The total batch size is 16 for all experiments. As shown in Figure 16, it is evident that SN-Netv2 exhibits significant improvement for stitches at low FLOPs, while also achieving competitive performance at high FLOPs. Notably, the highlighted Pareto frontier demonstrates that SN-Netv2 surpasses SN-Netv1 in terms of the overall performance-efficiency trade-offs.

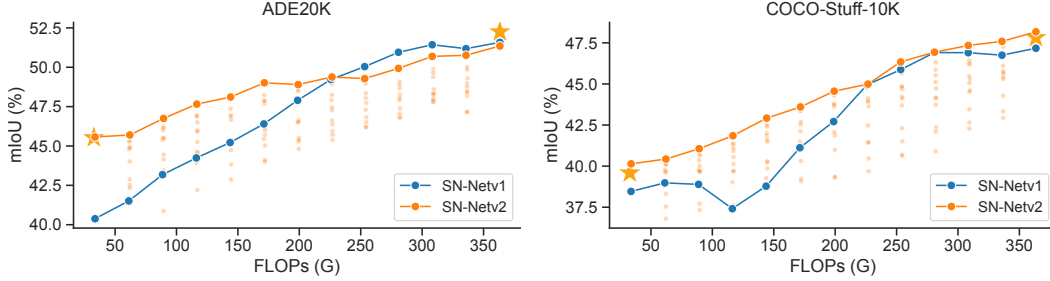


Figure 16: Performance comparison between SN-Netv1 and SN-Netv2 on ADE20K and COCO-Stuff-10K by stitching DeiT3-S and DeiT3-L.

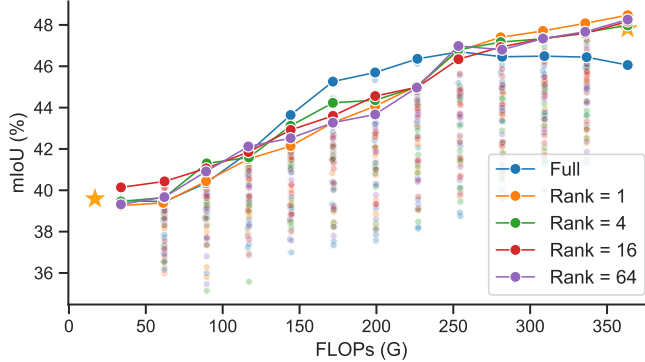


Figure 17: Effect of different ranks in LoRA SL based on stitching DeiT3-S and DeiT3-L on COCO-Stuff-10K. “Full” refers to fully finetune the stitching layers.

#### A.4 Effect of Different Ranks in LoRA SL

In Figure 17, we explore the effect of different ranks in LoRA SL by stitching DeiT3-S and DeiT3-L on COCO-Stuff-10K. In general, we observe that different low ranks perform similar, where they can effectively produce smoothly increasing Pareto frontiers. However, without the low-rank update, the performance of the stitches at the higher FLOPs drops (>250G FLOPs). Therefore, it indicates that low-rank update may regularize stitches learning during the training time.

#### A.5 Details of Benchmarked Pretrained ViTs

We have shown in Section 5.5 that different pretrained ViTs under SN-Netv2 performs differently due to the various training objectives and datasets. In this section, we provide the details of the benchmarked ViT weights.

- **DeiT3** [45]. ImageNet-21K pretrained DeiT3-B<sup>2</sup> and DeiT3-L<sup>3</sup>.
- **MAE** [20]. ImageNet-1K finetuned MAE-B<sup>4</sup> and MAE-L<sup>5</sup>.
- **SAM** [26]. SA-1B [26] pretrained SAM-B<sup>6</sup> and SAM-L<sup>7</sup>.
- **AugReg** [41]. ImageNet-21K pretrained and ImageNet-1K finetuned ViT-B<sup>8</sup> and ViT-L<sup>9</sup>.

<sup>2</sup>[https://dl.fbaipublicfiles.com/deit/deit\\_3\\_base\\_224\\_21k.pth](https://dl.fbaipublicfiles.com/deit/deit_3_base_224_21k.pth)

<sup>3</sup>[https://dl.fbaipublicfiles.com/deit/deit\\_3\\_large\\_224\\_21k.pth](https://dl.fbaipublicfiles.com/deit/deit_3_large_224_21k.pth)

<sup>4</sup>[https://dl.fbaipublicfiles.com/mae/finetune/mae\\_finnetuned\\_vit\\_base.pth](https://dl.fbaipublicfiles.com/mae/finetune/mae_finnetuned_vit_base.pth)

<sup>5</sup>[https://dl.fbaipublicfiles.com/mae/finetune/mae\\_finnetuned\\_vit\\_large.pth](https://dl.fbaipublicfiles.com/mae/finetune/mae_finnetuned_vit_large.pth)

<sup>6</sup>[https://dl.fbaipublicfiles.com/segment\\_anything/sam\\_vit\\_b\\_01ec64.pth](https://dl.fbaipublicfiles.com/segment_anything/sam_vit_b_01ec64.pth)

<sup>7</sup>[https://dl.fbaipublicfiles.com/segment\\_anything/sam\\_vit\\_l\\_0b3195.pth](https://dl.fbaipublicfiles.com/segment_anything/sam_vit_l_0b3195.pth)

<sup>8</sup>[https://huggingface.co/timm/vit\\_base\\_patch16\\_384.augreg\\_in21k\\_ft\\_in1k/blob/main/pytorch\\_model.bin](https://huggingface.co/timm/vit_base_patch16_384.augreg_in21k_ft_in1k/blob/main/pytorch_model.bin)

<sup>9</sup>[https://huggingface.co/timm/vit\\_large\\_patch16\\_384.augreg\\_in21k\\_ft\\_in1k/blob/main/pytorch\\_model.bin](https://huggingface.co/timm/vit_large_patch16_384.augreg_in21k_ft_in1k/blob/main/pytorch_model.bin)

- **BEiTv2 [34]**. ImageNet-1K pretrained, then ImageNet-21K finetuned, and finally ImageNet-1K finetuned BEiTv2-B<sup>10</sup> and BEiTv2-L<sup>11</sup>.

## References

- [1] Y. Bansal, P. Nakkiran, and B. Barak. Revisiting model stitching to compare neural representations. In *NeurIPS*, pages 225–236, 2021.
- [2] H. Bao, L. Dong, S. Piao, and F. Wei. Beit: BERT pre-training of image transformers. In *ICLR*, 2022.
- [3] T. Brown, B. Mann, N. Ryder, M. Subbiah, J. D. Kaplan, P. Dhariwal, A. Neelakantan, P. Shyam, G. Sastry, A. Askell, et al. Language models are few-shot learners. *NeurIPS*, 33:1877–1901, 2020.
- [4] H. Caesar, J. Uijlings, and V. Ferrari. Coco-stuff: Thing and stuff classes in context. In *CVPR*, pages 1209–1218, 2018.
- [5] M. Caron, H. Touvron, I. Misra, H. Jégou, J. Mairal, P. Bojanowski, and A. Joulin. Emerging properties in self-supervised vision transformers. In *ICCV*, 2021.
- [6] G. Chen, F. Liu, Z. Meng, and S. Liang. Revisiting parameter-efficient tuning: Are we really there yet? In *EMNLP*, 2022.
- [7] S. Chen, C. Ge, Z. Tong, J. Wang, Y. Song, J. Wang, and P. Luo. Adaptformer: Adapting vision transformers for scalable visual recognition. In *NeurIPS*, 2022.
- [8] X. Chen, S. Xie, and K. He. An empirical study of training self-supervised vision transformers. In *ICCV*, pages 9620–9629, 2021.
- [9] Z. Chen, Y. Duan, W. Wang, J. He, T. Lu, J. Dai, and Y. Qiao. Vision transformer adapter for dense predictions. In *ICLR*, 2023.
- [10] M. Contributors. MMSegmentation: Openmmlab semantic segmentation toolbox and benchmark. <https://github.com/open-mmlab/msegmentation>, 2020.
- [11] A. Csiszárík, P. Korösi-Szabó, Á. K. Matszangosz, G. Papp, and D. Varga. Similarity and matching of neural network representations. In *NeurIPS*, pages 5656–5668, 2021.
- [12] M. Dehghani, J. Djolonga, B. Mustafa, P. Padlewski, J. Heek, J. Gilmer, A. Steiner, M. Caron, R. Geirhos, I. Alabdulmohsin, et al. Scaling vision transformers to 22 billion parameters. *arXiv*, 2023.
- [13] X. Dong, J. Bao, T. Zhang, D. Chen, W. Zhang, L. Yuan, D. Chen, F. Wen, and N. Yu. Peco: Perceptual codebook for bert pre-training of vision transformers. In *AAAI*, 2023.
- [14] A. Dosovitskiy, L. Beyer, A. Kolesnikov, D. Weissenborn, X. Zhai, T. Unterthiner, M. Dehghani, M. Minderoeder, G. Heigold, S. Gelly, J. Uszkoreit, and N. Houlsby. An image is worth 16x16 words: Transformers for image recognition at scale. *ICLR*, 2021.
- [15] Y. Fang, W. Wang, B. Xie, Q. Sun, L. Wu, X. Wang, T. Huang, X. Wang, and Y. Cao. Eva: Exploring the limits of masked visual representation learning at scale. *arXiv*, 2022.
- [16] Y. Fang, S. Yang, S. Wang, Y. Ge, Y. Shan, and X. Wang. Unleashing vanilla vision transformer with masked image modeling for object detection. *arXiv*, 2022.
- [17] Z. Fu, H. Yang, A. M.-C. So, W. Lam, L. Bing, and N. Collier. On the effectiveness of parameter-efficient fine-tuning. *arXiv*, 2022.
- [18] P. Gao, T. Ma, H. Li, Z. Lin, J. Dai, and Y. Qiao. MCMAE: Masked convolution meets masked autoencoders. In *NeurIPS*, 2022.
- [19] M. Guo, C. Lu, Q. Hou, Z. Liu, M. Cheng, and S. Hu. Segnext: Rethinking convolutional attention design for semantic segmentation. In *NeurIPS*, 2022.
- [20] K. He, X. Chen, S. Xie, Y. Li, P. Dollár, and R. B. Girshick. Masked autoencoders are scalable vision learners. In *CVPR*, pages 15979–15988, 2022.
- [21] K. He, G. Gkioxari, P. Dollár, and R. Girshick. Mask r-cnn. In *ICCV*, pages 2961–2969, 2017.
- [22] Q. Hou, M. Cheng, X. Hu, A. Borji, Z. Tu, and P. H. S. Torr. Deeply supervised salient object detection with short connections. *TPAMI*, 41(4):815–828, 2019.
- [23] E. J. Hu, Y. Shen, P. Wallis, Z. Allen-Zhu, Y. Li, S. Wang, L. Wang, and W. Chen. Lora: Low-rank adaptation of large language models. In *ICLR*. OpenReview.net, 2022.

<sup>10</sup>[https://conversationhub.blob.core.windows.net/beit-share-public/beitv2/beitv2\\_base\\_patch16\\_224\\_pt1k\\_ft21kto1k.pth](https://conversationhub.blob.core.windows.net/beit-share-public/beitv2/beitv2_base_patch16_224_pt1k_ft21kto1k.pth)

<sup>11</sup>[https://conversationhub.blob.core.windows.net/beit-share-public/beitv2/beitv2\\_large\\_patch16\\_224\\_pt1k\\_ft21kto1k.pth](https://conversationhub.blob.core.windows.net/beit-share-public/beitv2/beitv2_large_patch16_224_pt1k_ft21kto1k.pth)

- [24] M. Jia, L. Tang, B.-C. Chen, C. Cardie, S. Belongie, B. Hariharan, and S.-N. Lim. Visual prompt tuning. In *ECCV*, pages 709–727, 2022.
- [25] J. Kaplan, S. McCandlish, T. Henighan, T. B. Brown, B. Chess, R. Child, S. Gray, A. Radford, J. Wu, and D. Amodei. Scaling laws for neural language models. *arXiv*, 2020.
- [26] A. Kirillov, E. Mintun, N. Ravi, H. Mao, C. Rolland, L. Gustafson, T. Xiao, S. Whitehead, A. C. Berg, W.-Y. Lo, P. Dollár, and R. Girshick. Segment anything. *arXiv*, 2023.
- [27] K. Lenc and A. Vedaldi. Understanding image representations by measuring their equivariance and equivalence. In *CVPR*, pages 991–999, 2015.
- [28] Y. Li, H. Mao, R. B. Girshick, and K. He. Exploring plain vision transformer backbones for object detection. In *ECCV*, 2022.
- [29] T. Lin, M. Maire, S. J. Belongie, J. Hays, P. Perona, D. Ramanan, P. Dollár, and C. L. Zitnick. Microsoft COCO: common objects in context. In D. J. Fleet, T. Pajdla, B. Schiele, and T. Tuytelaars, editors, *ECCV*, pages 740–755, 2014.
- [30] J. Liu, J. Cai, and B. Zhuang. Focusformer: Focusing on what we need via architecture sampler. *arXiv*, 2022.
- [31] Z. Liu, Y. Lin, Y. Cao, H. Hu, Y. Wei, Z. Zhang, S. Lin, and B. Guo. Swin transformer: Hierarchical vision transformer using shifted windows. In *ICCV*, pages 9992–10002, 2021.
- [32] M. Oquab, T. Darcet, T. Moutakanni, H. V. Vo, M. Szafraniec, V. Khalidov, P. Fernandez, D. Haziza, F. Massa, A. El-Nouby, R. Howes, P.-Y. Huang, H. Xu, V. Sharma, S.-W. Li, W. Galuba, M. Rabbat, M. Assran, N. Ballas, G. Synnaeve, I. Misra, H. Jegou, J. Mairal, P. Labatut, A. Joulin, and P. Bojanowski. Dinov2: Learning robust visual features without supervision. *arXiv*, 2023.
- [33] Z. Pan, J. Cai, and B. Zhuang. Stitchable neural networks. In *CVPR*, 2023.
- [34] Z. Peng, L. Dong, H. Bao, Q. Ye, and F. Wei. Beit v2: Masked image modeling with vector-quantized visual tokenizers. *arXiv*, 2022.
- [35] A. Radford, J. W. Kim, C. Hallacy, A. Ramesh, G. Goh, S. Agarwal, G. Sastry, A. Askell, P. Mishkin, J. Clark, G. Krueger, and I. Sutskever. Learning transferable visual models from natural language supervision. In *ICML*, pages 8748–8763, 2021.
- [36] A. Radford, J. Wu, R. Child, D. Luan, D. Amodei, I. Sutskever, et al. Language models are unsupervised multitask learners. *OpenAI blog*, 1(8):9, 2019.
- [37] R. Ranftl, A. Bochkovskiy, and V. Koltun. Vision transformers for dense prediction. In *ICCV*, pages 12179–12188, 2021.
- [38] O. Russakovsky, J. Deng, H. Su, J. Krause, S. Satheesh, S. Ma, Z. Huang, A. Karpathy, A. Khosla, M. Bernstein, et al. Imagenet large scale visual recognition challenge. *IJCV*, pages 211–252, 2015.
- [39] C. Schuhmann, R. Beaumont, R. Vencu, C. Gordon, R. Wightman, M. Cherti, T. Coombes, A. Katta, C. Mullis, M. Wortsman, et al. Laion-5b: An open large-scale dataset for training next generation image-text models. In *NeurIPS*, 2022.
- [40] N. Silberman, D. Hoiem, P. Kohli, and R. Fergus. Indoor segmentation and support inference from rgb-d images. In *ECCV*, pages 746–760, 2012.
- [41] A. P. Steiner, A. Kolesnikov, X. Zhai, R. Wightman, J. Uszkoreit, and L. Beyer. How to train your vit? data, augmentation, and regularization in vision transformers. *TMLR*, 2022.
- [42] R. Strudel, R. G. Pinel, I. Laptev, and C. Schmid. Segformer: Transformer for semantic segmentation. In *ICCV*, pages 7242–7252, 2021.
- [43] C. Sun, A. Shrivastava, S. Singh, and A. Gupta. Revisiting unreasonable effectiveness of data in deep learning era. In *ICCV*, pages 843–852, 2017.
- [44] H. Touvron, M. Cord, M. Douze, F. Massa, A. Sablayrolles, and H. Jégou. Training data-efficient image transformers & distillation through attention. In *ICML*, pages 10347–10357, 2021.
- [45] H. Touvron, M. Cord, and H. Jégou. Deit iii: Revenge of the vit. In *ECCV*, pages 516–533, 2022.
- [46] D. Wang, M. Li, C. Gong, and V. Chandra. Attention-venas: Improving neural architecture search via attentive sampling. In *CVPR*, pages 6418–6427, 2021.
- [47] Y. Wu, A. Kirillov, F. Massa, W.-Y. Lo, and R. Girshick. Detectron2. <https://github.com/facebookresearch/detectron2>, 2019.
- [48] Z. Wu, L. Su, and Q. Huang. Cascaded partial decoder for fast and accurate salient object detection. In *CVPR*, pages 3907–3916, 2019.
- [49] E. Xie, W. Wang, Z. Yu, A. Anandkumar, J. M. Alvarez, and P. Luo. Segformer: Simple and efficient design for semantic segmentation with transformers. In *NeurIPS*, pages 12077–12090, 2021.



- [50] Z. Xie, Z. Zhang, Y. Cao, Y. Lin, J. Bao, Z. Yao, Q. Dai, and H. Hu. Simmim: A simple framework for masked image modeling. In *CVPR*, pages 9653–9663, 2022.
- [51] X. Yang, D. Zhou, S. Liu, J. Ye, and X. Wang. Deep model reassembly. *NeurIPS*, 2022.
- [52] J. Yu, Z. Wang, V. Vasudevan, L. Yeung, M. Seyedhosseini, and Y. Wu. Coca: Contrastive captioners are image-text foundation models. *arXiv*, 2022.
- [53] X. Zhai, A. Kolesnikov, N. Houlsby, and L. Beyer. Scaling vision transformers. In *CVPR*, pages 12104–12113, 2022.
- [54] B. Zhang, Z. Tian, Q. Tang, X. Chu, X. Wei, C. Shen, and Y. Liu. Segvit: Semantic segmentation with plain vision transformers. In *NeurIPS*, 2022.
- [55] S. Zhang, S. Roller, N. Goyal, M. Artetxe, M. Chen, S. Chen, C. Dewan, M. Diab, X. Li, X. V. Lin, et al. Opt: Open pre-trained transformer language models. *Arxiv*, 2022.
- [56] S. Zheng, J. Lu, H. Zhao, X. Zhu, Z. Luo, Y. Wang, Y. Fu, J. Feng, T. Xiang, P. H. Torr, et al. Rethinking semantic segmentation from a sequence-to-sequence perspective with transformers. In *CVPR*, pages 6881–6890, 2021.
- [57] B. Zhou, H. Zhao, X. Puig, S. Fidler, A. Barriuso, and A. Torralba. Scene parsing through ade20k dataset. In *CVPR*, pages 633–641, 2017.
- [58] J. Zhou, C. Wei, H. Wang, W. Shen, C. Xie, A. L. Yuille, and T. Kong. Image BERT pre-training with online tokenizer. In *ICLR*, 2022.